Phys Chem Minerals (2003) 30: 167–176
DOI 10.1007/s00269-003-0303-9

ORIGINAL PAPER

R. J. Angel · C. S. J. Shaw · G. V. Gibbs

Compression mechanisms of coesite

Received: 11 July 2002 / Accepted: 14 January 2003

Abstract The structure of coesite has been determined at ten pressures up to a maximum of 8.68 GPa by single-crystal X-ray diffraction. The dominant mechanism of compression is the reduction of four of the five independent Si–O–Si angles within the structure. There is no evidence of the fifth linkage, Si1–O1–Si1, deviating from 180°. Some Si–O bond distances also decrease by up to 1.6% over the pressure range studied. The pattern of Si–O–Si angle reduction amounts to a rotation of the Si2 tetrahedron around the [001] direction. This rotation induces significant internal deformation of the Si1 tetrahedron. Comparison of the experimental data with rigid-unit distance least-squares simulations of coesite suggests that this pattern of compression, the anomalous positive values of both s_{23} and K″ in the equation of state of coesite, its high elastic anisotropy and the unusual straight Si1–O1–Si1 linkage within the structure are all consequences of the connectivity of the tetrahedral framework.

Keywords Coesite · Structure · High pressure · Compression mechanisms

Introduction

Understanding the thermodynamics and physical properties of coesite has become increasingly important as it is discovered in more ultrahigh-pressure terraines in which it is a critical pressure marker (e.g. Chopin 1983; Parkinson and Katayama 1999; Parkinson 2000; O'Brien et al. 2001). However, the elastic properties of coesite are very anomalous in several respects (Angel et al. 2001b). First, the second derivative of the bulk modulus is significantly positive, whereas it is normally slightly negative in most materials. Second, the *c*-cell edge appears to undergo about 10% softening upon hydrostatic compression of the structure up to ~3 GPa, after which it displays more normal behaviour of increasing stiffness with further increase in pressure. Both of these anomalies are presumably related to the unusual positive value for one of the off-diagonal components, s_{23}, of the elastic compliance tensor of coesite (Weidner and Carleton 1977) when it is described in the coordinate system x // **a***, y // **b**, z // **c**. The positive value of s_{23} means that uniaxial compression of the *b*-cell edge leads to uniaxial compression of the *c*-cell edge, and viceversa. This contrasts with the behaviour of most materials in which these off-diagonal terms are positive, which corresponds to a positive Poisson ratio, and compression of any one direction leads to expansion in perpendicular directions.

Coesite has a structure comprised of SiO_4 tetrahedra that are fully polymerized into a three-dimensional framework. The topology of the framework is related to that of feldspar (Megaw 1970). Both frameworks are comprised of four-membered rings of tetrahedra that form chains that run parallel to the *c*-cell edge of the unit cell, and the linkages between these chains of 4-rings are such that crankshaft-like chains are formed. The different space groups of the feldspar structure ($C2/m$) and that of coesite ($C2/c$) result in the crankshaft chains being parallel to [100] in feldspar and [101] in coesite (Fig. 1). Megaw (1970) discusses the relationship between the two structure types in more detail. Feldspars, however, are stable at ambient conditions, whereas coesite is only thermodynamically stable at high pressures. A simple-minded explanation of the anomalous elastic properties of coesite would be that, as a high-pressure phase, its framework is overexpanded at room pressure. If so, then one would expect that initial rapid

R. J. Angel (✉) · G. V. Gibbs
Crystallography Laboratory,
Dept. Geological Sciences, Virginia Tech,
Blacksburg, Virginia 24060, USA
e-mail: rangel@vt.edu
Tel.: +540-231-7974
Fax: +540-231-3386

C. S. J. Shaw
Department of Geology,
University of New Brunswick, 2 Bailey Drive,
Fredericton, New Brunswick, E3B 5A3, Canada

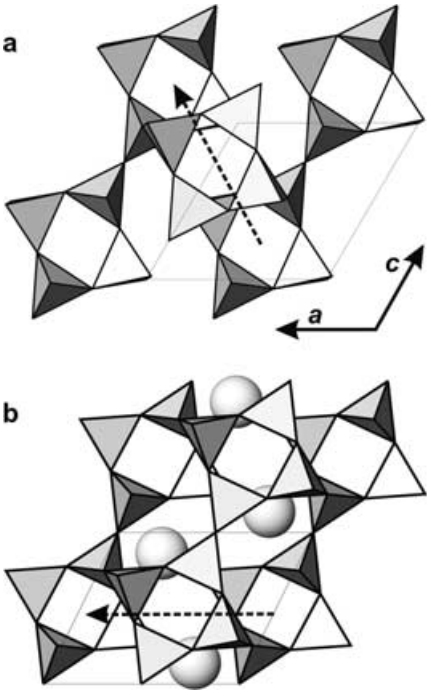

Fig. 1a,b Polyhedral representations of the structures of **a** coesite and **b** feldspar viewed down the *b*-cell edge. The crankshaft chains of the four-rings of tetrahedra run parallel to [101] in coesite and [100] in feldspar, as indicated by the *dashed arrows*. The positions of the alkali atoms in the feldspar structure are shown by the *spheres*

compression would occur until the structure was returned to a more "normal" configuration, presumably around 3 GPa, after which it would display more "normal" compressional behaviour and elasticity, typical of that of polyhedral frameworks. The previous high-pressure structural data for coesite extended to 5.2 GPa (Levien and Prewitt 1981), but showed no obvious changes in patterns of compression that could be correlated with the unusual behaviour of its equation of state. We have therefore undertaken a single-crystal X-ray diffraction study of coesite to higher pressures in the hope that the wider range of pressure would enable the underlying structural reasons for the anomalous elastic properties to be detected.

Experimental

Two single crystals were used for structure determination at high pressure in two separate loadings of a diamond-anvil cell. Both crystals were selected from the products of the same synthesis designated as CS45 in Angel et al. (2001b), where the details of synthesis are described. Both crystals, denoted X1 and X4, were in the form of plates approximately parallel to (14-1), an orientation that provides approximately equal resolution along all three reciprocal lattice axes when the crystals are mounted in a transmission-type diamond-anvil cell. Diamond-anvil cells (DACs) of the BGI design were used (Allan et al. 1996) with rhenium gaskets and a 4:1 methanol:ethanol mixture as the pressure medium. A quartz crystal was included with the crystal X1 in the pressure cell as an internal diffraction standard and pressure was determined from the equation of state of quartz (Angel et al. 1997). In an attempt to improve the signal-to-noise ratio of the intensity datasets, crystal X4 was larger than X1 and, to provide sufficient room in the chamber of the DAC, no quartz crystal was included. Instead, pressures were estimated from the β unit-cell angle of the X4 crystal and the variation of β with pressure previously determined for crystal X1 (Angel et al. 2001b).

Unit-cell parameters of the coesite at each pressure were determined by diffraction on a Huber four-circle diffractometer driven by the Single software (Angel et al. 2001a). The software employs eight-position centering of diffraction maxima (King and Finger 1979) to eliminate the effect of diffractometer aberrations and crystal offsets, and vector-least-squares fitting of the unit-cell parameters (Ralph and Finger 1982). Intensity datasets were recorded with MoKα radiation on a CAD4 diffractometer operated in fixed-phi mode (Finger and King 1978). All accessible reflections allowed by the $C2/c$ symmetry of coesite up to 80° 2theta were collected with omega scans in a constant precision mode, with a maximum scan time per peak of 450 s. In addition, a dataset was also collected from the X1 crystal mounted on a glass fibre, prior to it being loaded in the DAC. Integrated intensities were obtained from the step-scan data by fitting a pre-determined peak function to the α_1–α_2 doublet of each reflection with the WinIntegrStp program (Angel 2003). Integrated intensities were then corrected for Lorentz and polarization effects and the absorption by the crystal and by the components of the DAC with the ABSORB program (Burnham 1966; Angel 2002). Total transmission factors typically ranged from ~0.27 to ~0.36. Averaged structure factors were then obtained by averaging symmetry-equivalent reflections in Laue group $2/m$ following the criteria recommended by Blessing (1987).

Structure refinements were carried out with RFINE99, a development version of RFINE-4 (Finger and Prince 1974), using the coefficients for scattering factors of neutral atoms and dispersion corrections from the International Tables for Crystallography (Maslen et al. 1992; Creagh and McAuley 1992), using reflections with $F > 4\sigma(F)$. Final refinements were carried out with anisotropic displacement parameters for all atoms. For the refinement of the datasets X1P8 and X1P3 the β_{22} of the O5 atom was constrained to the value determined at room pressure in order to maintain a positive-definite displacement ellipsoid for this one atom. All refinements also included a refined coefficient for extinction (Lorentzian type I distribution: Becker and Coppens 1974). At convergence of each refinement the data were examined for outliers as defined as those reflections with large values of $|F_{obs} - F_{calc}|/\delta(F_{obs})$. In DAC experiments with low-symmetry crystals such as coesite these can easily arise from unidentified diffraction effects in the DAC. In each refinement a few outliers, typically four to six in number, were then excluded in the final refinement. If the slope of the normal probability plot of the data (Abrahams and Keve 1971) then exceeded unity at convergence of the subsequent refinement, the weights for the reflections in the final cycles of refinement were adjusted by a factor p in weight $= \left[\sigma_i^2(F_i) + p^2F_i^2\right]^{-2}$ so as to obtain a slope of unity. Final refinement indices are given in Table 1, refined positional and displacement parameters in Table 2, and selected bond lengths and angles in Table 3.

Two types of distance-least-squares simulations were performed with the DLS-76 program (Baerlocher et al. 1977) in order to simulate the behaviour of the coesite tetrahedral framework with the aim of identifying the features and properties of the structure that are the most important in determining its behaviour. We performed a DLS simulation corresponding to each of the experimental data points. For each simulation the unit-cell parameters were constrained to those measured experimentally at that pressure, but the internal dimensions of the tetrahedra (O-Si–O angles and Si–O distances) were constrained to remain equal to those measured at room pressure. No constraints were assigned to the Si–O–Si angles (or to the Si–Si distances) in these DLS simulations. The resulting simulated structures therefore represent the compressional behaviour of a framework consisting of rigid tetrahedral units, and we therefore refer to this as the rigid-unit simulation. Deviations of the experimentally determined structures from this

Table 1 Refinement indices. Pressures for crystal X1 were determined from the unit-cell volumes of a quartz crystal included in the diamond-anvil cell. Pressures for crystal X4 were estimated from the β unit-cell angle of the coesite crystal. In coesite there are 16 refinable positional parameters and 40 refinable anisotropic displacement parameters (Table 2). The scale and extinction parameters were refined for the X1 datasets, and thus *Npar* is 58, except for datasets X1P8 and X1P3 in which β_{22} of oxygen O5 was constrained to be equal to the value determined in X1P0 in order to obtain a positive-definite displacement ellipsoid. For crystal X4, the extinction parameter refined to less than its esd, so it was excluded from the final refinements and the number of parameters, *Npar*, is thus 57

	P: GPa	*N*obs	*R*u	*R*w	*G*fit	*N*par
X1air	10^{-4}	1415	0.036	0.048	1.34	58
X1P0	10^{-4}	429	0.029	0.034	1.19	58
X1P8	2.248(6)	418	0.032	0.037	1.18	57
X4P4	2.84(4)	415	0.032	0.033	1.16	57
X1P3	3.763(5)	397	0.030	0.035	1.13	57
X4P2	4.45(4)	410	0.033	0.039	1.21	57
X4P3	5.01(4)	403	0.032	0.032	1.06	57
X1P12	6.16(4)	395	0.032	0.038	1.15	58
X1P5	6.509(6)	400	0.033	0.040	1.17	58
X1P7	7.814(11)	393	0.034	0.038	1.18	58
X4P1	8.68(4)	398	0.034	0.040	1.25	57

model presumably represent the effects of angular deformation of the tetrahedra (i.e., changes in O-Si–O angles) and/or compression of the Si–O bonds.

The second set of DLS simulations was performed in order to understand the elastic anisotropy of coesite at room pressure alone. In these simulations some of the unit-cell parameters were refined. In order to compensate for this increase in the degrees of freedom and to obtain stable convergence in this simulation, it was found necessary to additionally constrain the Si–Si distances to the values observed at room pressure.

Results

The crystal structure refined to the data collected from the X1 crystal in air is essentially identical to those reported by Geisinger et al. (1987), Downs (1995) and Levien and Prewitt (1981). In detail, the Si–O bond lengths and the Si–O–Si bond angles for the structure determined in the current study (Table 3) are identical within the mutual standard uncertainties, msu, to those determined by Downs (1995), and the O–Si–O angles differ by up to two msu. The differences between the current refined structure and that of Levien and Prewitt (1981) are slightly larger, but remain less than 0.003 Å for any Si–O bond length and 0.2° for Si–O–Si and O–Si–O angles. The refined anisotropic displacement parameters in our room-pressure refinement represent differences in mean-squares displacements of O atoms towards Si and Si towards O of less than 4%, and are therefore consistent with rigid-body motion of the SiO_4 tetrahedra.

There are differences of up to 0.003 Å in Si–O bond lengths, 0.16° in Si–O–Si angles and 0.3° in O–Si–O angles (Table 3) between the structure refined to the dataset collected in air (X1air) and that collected at room pressure in the DAC (X1P0). None of these differences exceeds 3 msu, and most are less than 2 msu. Nonetheless, the differences indicate that that not all of the effects of the diamond cell on the intensity dataset have been eliminated in the data reduction process. This is more apparent when the displacement parameters are examined (Table 2); but the structure refinements to a series of datasets collected from the same crystal mount at various high pressures can reasonably be expected to suffer the same systematic errors. Therefore, in order to identify the changes occurring in the structure of coesite during compression, the structure refined to the dataset X1P0 will be used as the room-pressure reference in all of the following discussion. Note also that the restricted access to reflections in the DAC (Table 1) contributes to the larger estimated standard deviations (esd) in the parameters at high pressure because the number of observations used in the least-squares refinement is reduced by a factor of approximately 3.

In general, the trends in the coesite structure that we observe up to 5.2 GPa are very similar to those reported by Levien and Prewitt (1981), and these trends appear to continue smoothly to 8.7 GPa. There is also close agreement between our experimental results and the first-principles calculations by Gibbs et al. (2000) that suggest that these trends continue smoothly to higher pressures. In particular, there are no obvious or discontinuous changes in the compression mechanisms around 3 GPa, above which pressure the compression curve of coesite ceases to be anomalous (Angel et al. 2001b). As a framework consisting of corner-linked SiO_4 tetrahedra, the most obvious structural change that occurs upon compression is the reduction of the Si–O–Si bond angles (Fig. 2). However, the pattern of change in these angles is contrary to that expected in that the smaller angles undergo the most compression. The largest Si–O–Si bond angle at room pressure is that at O1, which is constrained to be 180° by the location of O1 on the centre of symmetry at the origin of the unit cell. Such linear linkages have been the subject of much discussion and controversy in the literature. Many have been shown to represent a time average of an Si–O–Si linkage with a normal bond angle and the oxygen atom executing a precession motion around the Si–Si vector (e.g. cristobalite; Swainson and Dove 1995). Others appear to be the result of spatial averaging of statically disordered linkages with normal Si–O–Si angles. In these cases, the disorder is reflected in the anisotropic displacement parameters of the bridging oxygen atom. Such is not the case in coesite at room pressure, because the displacement parameters for the O1 oxygen are small and typical of those for the other four symmetrically distinct oxygen positions within the structure (Table 2). The link therefore appears to be truly linear, consistent with NMR studies (Grandinetti et al. 1995) of coesite. There are no changes in the displacement parameters of O1 at elevated pressures, at least within the larger uncertainties associated with data collected from a crystal in a DAC. Nor is there any evidence of symmetry-breaking in the form of either increased discrepancy

Table 2 Refined positional and displacement parameters for coesite

Atom	*x*	*y*	*z*	$\beta 11$	$\beta 22$	$\beta 33$	$\beta 12$	$\beta 13$	$\beta 23$	Beq/Biso
Refined positional and displacement parameters for X1air (room pressure, outside of DAC) Unit-cell parameters: 7.1366 12.3723 7.1749 90.000 120.330 90.000										
Si1	0.14023 (8)	0.10836 (4)	0.07236 (8)	0.00373 (10)	0.00069 (3)	0.00380 (9)	−0.00024 (4)	0.00182 (8)	−0.00013 (4)	0.531
Si2	0.50676 (8)	0.15804 (4)	0.54067 (7)	0.00418 (10)	0.00080 (3)	0.00357 (9)	−0.00009 (4)	0.00210 (8)	−0.00003 (4)	0.548
O1	0.0000	0.0000	0.0000	0.0058 (4)	0.00090 (7)	0.0069 (4)	−0.00108 (13)	0.0031 (3)	−0.00067 (13)	0.840
O2	0.5000	0.11637 (13)	0.7500	0.0067 (4)	0.00143 (8)	0.0039 (3)	0.0000	0.0034 (3)	0.0000	0.784
O3	0.2663 (3)	0.12316 (10)	0.9402 (2)	0.0056 (3)	0.00157 (6)	0.0066 (3)	−0.00057 (10)	0.0042 (3)	−0.00010 (10)	0.868
O4	0.3110 (3)	0.10382 (9)	0.3280 (2)	0.0066 (3)	0.00152 (6)	0.0036 (3)	−0.00068 (10)	0.0013 (2)	−0.00045 (10)	0.923
O5	0.0173 (3)	0.21194 (10)	0.4789 (2)	0.0058 (3)	0.00074 (5)	0.0076 (3)	−0.00004 (9)	0.0033 (3)	0.00015 (10)	0.840
Refined positional and displacement parameters for X1P0 (room pressure) Unit-cell parameters: 7.1366 12.3723 7.1749 90.000 120.330 90.000										
Si1	0.14051 (12)	0.10831 (9)	0.07236 (13)	0.00290 (16)	0.00056 (12)	0.0030 (3)	−0.00038 (8)	0.00171 (14)	−0.00025 (7)	0.40 (2)
Si2	0.50679 (12)	0.15828 (9)	0.54093 (13)	0.00332 (15)	0.00095 (12)	0.0021 (3)	−0.00012 (8)	0.00174 (13)	−0.00002 (7)	0.443 (19)
O1	0.0000	0.0000	0.0000	0.0043 (6)	0.0012 (5)	0.0043 (9)	−0.0009 (4)	0.0017 (6)	−0.0008 (3)	0.72 (7)
O2	0.5000	0.1165 (3)	0.7500	0.0048 (6)	0.0007 (5)	0.0044 (10)	0.0000	0.0027 (6)	0.0000	0.58 (6)
O3	0.2662 (3)	0.1233 (3)	0.9411 (4)	0.0051 (5)	0.0014 (3)	0.0050 (6)	−0.0003 (3)	0.0034 (4)	−0.0003 (3)	0.73 (5)
O4	0.3110 (4)	0.1039 (3)	0.3275 (4)	0.0065 (5)	0.0016 (4)	0.0026 (7)	−0.0005 (3)	0.0009 (4)	−0.00036 (19)	0.87 (5)
O5	0.0175 (4)	0.2124 (3)	0.4787 (4)	0.0051 (4)	0.0004 (4)	0.0072 (8)	−0.0002 (3)	0.0030 (4)	−0.0002 (2)	0.71 (5)
Refined positional and displacement parameters for X1P8 (2.248 GPa) Unit-cell parameters: 7.0666 12.3049 7.1462 90.000 120.540 90.000										
Si1	0.13863 (12)	0.10913 (9)	0.07124 (13)	0.00331 (17)	0.00095 (13)	0.0025 (3)	−0.00043 (8)	0.00152 (14)	−0.00029 (8)	0.48 (3)
Si2	0.50784 (11)	0.15750 (9)	0.54297 (13)	0.00358 (16)	0.00098 (13)	0.0026 (3)	0.00004 (9)	0.00182 (14)	−0.00002 (7)	0.48 (3)
O1	0.0000	0.0000	0.0000	0.0058 (6)	0.0005 (5)	0.0063 (9)	−0.0014 (4)	0.0016 (6)	−0.0009 (3)	0.81 (6)
O2	0.5000	0.1128 (3)	0.7500	0.0053 (6)	0.0011 (5)	0.0038 (10)	0.0000	0.0022 (6)	0.0000	0.69 (6)
O3	0.2599 (3)	0.1266 (3)	0.9349 (4)	0.0048 (5)	0.0009 (4)	0.0063 (7)	−0.0007 (3)	0.0032 (4)	−0.0005 (3)	0.71 (5)
O4	0.3142 (3)	0.1023 (3)	0.3265 (4)	0.0059 (5)	0.0011 (4)	0.0036 (7)	−0.0005 (3)	0.0011 (4)	−0.0010 (3)	0.78 (5)
O5	0.0226 (4)	0.2117 (3)	0.4749 (4)	0.0053 (5)	0.0004	0.0070 (6)	0.0000 (3)	0.0030 (4)	0.0002 (2)	0.70 (4)
Refined positional and displacement parameters for X4P4 (2.84 GPa) Unit-cell parameters: 7.0500 12.2907 7.1386 90.000 120.587 90.000										
Si1	0.13849 (17)	0.10936 (7)	0.07116 (14)	0.0032 (6)	0.00061 (8)	0.0028 (3)	−0.00029 (7)	0.0020 (4)	−0.00022 (7)	0.39 (2)
Si2	0.50819 (17)	0.15731 (7)	0.54319 (14)	0.0035 (6)	0.00072 (8)	0.0026 (3)	−0.00002 (7)	0.0022 (4)	−0.00004 (7)	0.40 (2)
O1	0.0000	0.0000	0.0000	0.005 (3)	0.0007 (3)	0.0052 (9)	−0.0007 (3)	0.0019 (13)	−0.0004 (3)	0.68 (7)
O2	0.5000	0.1117 (3)	0.7500	0.007 (2)	0.0010 (3)	0.0046 (10)	0.0000	0.0044 (13)	0.0000	0.71 (7)
O3	0.2575 (5)	0.12731 (17)	0.9322 (4)	0.0015 (14)	0.0017 (2)	0.0042 (7)	−0.00027 (19)	0.0016 (9)	−0.0001 (2)	0.61 (5)
O4	0.3158 (5)	0.10222 (17)	0.3264 (4)	0.0048 (14)	0.0013 (2)	0.0031 (7)	−0.00044 (19)	0.0010 (9)	−0.0006 (2)	0.73 (5)
O5	0.0236 (5)	0.21242 (17)	0.4743 (4)	0.0050 (13)	0.0006 (2)	0.0066 (7)	−0.00019 (18)	0.0039 (9)	0.00036 (19)	0.64 (5)
Refined positional and displacement parameters for X1P3 (3.763 GPa) Unit-cell parameters: 7.0203 12.2615 7.1260 90.000 120.670 90.000										
Si1	0.13760 (12)	0.10979 (9)	0.07067 (13)	0.00354 (17)	0.00082 (13)	0.0027 (3)	−0.00025 (8)	0.00177 (14)	−0.00014 (8)	0.46 (3)
Si2	0.50850 (12)	0.15724 (9)	0.54405 (13)	0.00351 (17)	0.00060 (13)	0.0028 (3)	−0.00022 (8)	0.00171 (14)	−0.00011 (7)	0.42 (3)
O1	0.0000	0.0000	0.0000	0.0054 (7)	0.0007 (5)	0.0061 (9)	−0.0009 (4)	0.0021 (6)	0.0000 (4)	0.77 (7)
O2	0.5000	0.1108 (3)	0.7500	0.0056 (6)	0.0012 (5)	0.0032 (9)	0.0000	0.0033 (6)	0.0000	0.61 (7)
O3	0.2558 (3)	0.12881 (19)	0.9309 (4)	0.0052 (5)	0.0011 (4)	0.0050 (7)	0.0000 (3)	0.0030 (4)	0.0001 (3)	0.71 (5)
O4	0.3174 (3)	0.1011 (3)	0.3262 (4)	0.0060 (5)	0.0009 (4)	0.0038 (7)	−0.0003 (3)	0.0011 (4)	−0.0007 (3)	0.75 (5)
O5	0.0253 (4)	0.2120 (3)	0.4721 (4)	0.0049 (5)	0.0004	0.0072 (6)	−0.0003 (3)	0.0032 (4)	0.0001 (3)	0.67 (4)
Refined positional and displacement parameters for X4P2 (4.45 GPa) Unit-cell parameters: 7.0035 12.2462 7.1178 90.000 120.708 90.000										
Si1	0.13737 (18)	0.11000 (8)	0.07059 (16)	0.0033 (6)	0.00064 (8)	0.0026 (3)	−0.00024 (7)	0.0018 (4)	−0.00019 (8)	0.39 (2)
Si2	0.50834 (18)	0.15720 (8)	0.54402 (15)	0.0042 (6)	0.00079 (9)	0.0019 (3)	0.00009 (8)	0.0021 (4)	0.00001 (8)	0.42 (3)
O1	0.0000	0.0000	0.0000	0.007 (3)	0.0006 (4)	0.0059 (10)	−0.0006 (3)	0.0037 (13)	−0.0001 (4)	0.70 (7)
O2	0.5000	0.1098 (3)	0.7500	0.005 (3)	0.0012 (3)	0.0022 (10)	0.0000	0.0022 (13)	0.0000	0.53 (7)
O3	0.2538 (5)	0.12928 (18)	0.9293 (5)	0.0042 (14)	0.0015 (3)	0.0054 (8)	−0.0003 (3)	0.0033 (10)	−0.0001 (3)	0.70 (5)
O4	0.3180 (5)	0.10101 (19)	0.3254 (5)	0.0046 (15)	0.0015 (3)	0.0032 (8)	−0.00029 (19)	0.0011 (9)	−0.0003 (2)	0.73 (5)
O5	0.0259 (5)	0.21265 (18)	0.4715 (5)	0.0054 (14)	0.0008 (3)	0.0063 (8)	0.00009 (19)	0.0037 (9)	0.0002 (3)	0.68 (5)
Refined positional and displacement parameters for X4P3 (5.01 GPa) Unit-cell parameters: 6.9862 12.2311 7.1101 90.000 120.746 90.000										
Si1	0.13687 (17)	0.11026 (7)	0.07002 (14)	0.0029 (6)	0.00064 (8)	0.0023 (3)	−0.00025 (7)	0.0015 (4)	−0.00027 (7)	0.370 (18)
Si2	0.50836 (16)	0.15706 (7)	0.54447 (14)	0.0037 (6)	0.00078 (8)	0.0020 (3)	−0.00005 (7)	0.0018 (4)	−0.00008 (7)	0.405 (19)
O1	0.0000	0.0000	0.0000	0.007 (3)	0.0003 (3)	0.0062 (10)	−0.0002 (3)	0.0040 (13)	0.0001 (3)	0.67 (7)
O2	0.5000	0.1093 (3)	0.7500	0.005 (2)	0.0013 (3)	0.0026 (9)	0.0000	0.0031 (12)	0.0000	0.56 (6)
O3	0.2523 (5)	0.13006 (15)	0.9278 (4)	0.0068 (15)	0.00115 (19)	0.0052 (7)	−0.00051 (19)	0.0045 (10)	−0.0002 (2)	0.72 (5)
O4	0.3189 (5)	0.10058 (17)	0.3252 (4)	0.0069 (13)	0.00136 (19)	0.0036 (7)	−0.0003 (2)	0.0022 (8)	−0.00043 (19)	0.81 (5)
O5	0.0267 (5)	0.21270 (17)	0.4707 (4)	0.0047 (13)	0.0009 (2)	0.0068 (7)	0.00007 (18)	0.0040 (9)	0.00042 (18)	0.68 (5)

Table 2 (Contd.)

Atom	*x*	*y*	*z*	$\beta 11$	$\beta 22$	$\beta 33$	$\beta 12$	$\beta 13$	$\beta 23$	Beq/Biso
Refined positional and displacement parameters for X1P12 (6.16 GPa)										
Unit-cell parameters: 6.9520	12.1986	7.0942	90.000	120.820	90.000					
Si1	0.13588 (12)	0.11051 (8)	0.06934 (15)	0.00362 (17)	0.00088 (13)	0.0038 (4)	−0.00021 (8)	0.00195 (16)	−0.00026 (8)	0.53 (2)
Si2	0.50905 (13)	0.15687 (9)	0.54548 (15)	0.00402 (17)	0.00092 (13)	0.0032 (4)	−0.00010 (8)	0.00193 (15)	−0.00008 (8)	0.52 (3)
O1	0.0000	0.0000	0.0000	0.0065 (7)	0.0009 (5)	0.0076 (12)	−0.0008 (4)	0.0034 (7)	−0.0004 (4)	0.88 (6)
O2	0.5000	0.1074 (4)	0.7500	0.0072 (7)	0.0014 (5)	0.0035 (13)	0.0000	0.0030 (7)	0.0000	0.78 (6)
O3	0.2499 (4)	0.1314 (3)	0.9245 (5)	0.0049 (5)	0.0015 (3)	0.0054 (8)	−0.0004 (3)	0.0033 (5)	−0.0002 (3)	0.75 (4)
O4	0.3205 (4)	0.1006 (3)	0.3247 (4)	0.0068 (5)	0.0014 (4)	0.0041 (9)	−0.0004 (3)	0.0020 (5)	−0.0004 (3)	0.86 (5)
O5	0.0291 (4)	0.2117 (3)	0.4706 (4)	0.0059 (5)	0.0009 (3)	0.0065 (9)	−0.0002 (3)	0.0038 (5)	0.0000 (2)	0.73 (5)
Refined positional and displacement parameters for X1P5 (6.509 GPa)										
Unit-cell parameters: 6.9450	12.1909	7.0912	90.000	120.850	90.000					
Si1	0.13572 (12)	0.11079 (9)	0.06913 (14)	0.00347 (18)	0.00076 (15)	0.0028 (3)	−0.00023 (9)	0.00195 (15)	−0.00018 (8)	0.43 (3)
Si2	0.50923 (12)	0.15689 (10)	0.54560 (13)	0.00328 (18)	0.00084 (15)	0.0028 (3)	−0.00022 (9)	0.00178 (15)	−0.00019 (7)	0.44 (3)
O1	0.0000	0.0000	0.0000	0.0069 (7)	0.0004 (5)	0.0055 (10)	−0.0007 (4)	0.0022 (6)	−0.0001 (4)	0.74 (7)
O2	0.5000	0.1076 (4)	0.7500	0.0064 (7)	0.0013 (6)	0.0030 (10)	0.0000	0.0031 (6)	0.0000	0.66 (8)
O3	0.2495 (4)	0.1314 (3)	0.9242 (4)	0.0048 (5)	0.0016 (4)	0.0042 (7)	−0.0002 (3)	0.0032 (4)	0.0001 (3)	0.70 (5)
O4	0.3207 (4)	0.1005 (3)	0.3253 (4)	0.0061 (5)	0.0011 (4)	0.0037 (7)	0.0001 (3)	0.0015 (4)	−0.0004 (3)	0.76 (5)
O5	0.0298 (4)	0.2121 (3)	0.4693 (4)	0.0050 (5)	0.0006 (4)	0.0061 (7)	−0.0004 (3)	0.0030 (4)	−0.0002 (3)	0.66 (5)
Refined positional and displacement parameters for X1P7 (7.814 GPa)										
Unit-cell parameters: 6.9126	12.1610	7.0746	90.000	120.910	90.000					
Si1	0.13505 (13)	0.11103 (9)	0.06876 (14)	0.00356 (19)	0.00074 (14)	0.0031 (3)	−0.00027 (9)	0.00195 (16)	−0.00027 (8)	0.45 (3)
Si2	0.50932 (13)	0.15664 (9)	0.54624 (14)	0.00366 (18)	0.00064 (13)	0.0031 (3)	−0.00015 (10)	0.00205 (16)	−0.00018 (8)	0.43 (2)
O1	0.0000	0.0000	0.0000	0.0059 (8)	0.0014 (5)	0.0046 (10)	−0.0008 (4)	0.0019 (7)	−0.0003 (4)	0.83 (7)
O2	0.5000	0.1062 (3)	0.7500	0.0061 (7)	0.0006 (5)	0.0050 (11)	0.0000	0.0038 (6)	0.0000	0.59 (6)
O3	0.2470 (4)	0.1328 (3)	0.9217 (4)	0.0047 (5)	0.0021 (4)	0.0034 (8)	0.0001 (3)	0.0031 (5)	0.0000 (3)	0.74 (5)
O4	0.3218 (4)	0.1000 (3)	0.3239 (4)	0.0062 (5)	0.0015 (4)	0.0028 (8)	−0.0002 (3)	0.0015 (5)	−0.0005 (3)	0.77 (5)
O5	0.0318 (4)	0.2125 (3)	0.4692 (4)	0.0055 (5)	0.0010 (4)	0.0058 (8)	−0.0001 (3)	0.0035 (5)	−0.0001 (3)	0.71 (5)
Refined positional and displacement parameters for X4P1 (8.68 GPa)										
Unit-cell parameters: 6.8886	12.1377	7.0625	90.000	120.962	90.000					
Si1	0.1347 (2)	0.11137 (7)	0.06850 (16)	0.0035 (6)	0.00054 (9)	0.0026 (3)	−0.00010 (8)	0.0019 (4)	−0.00012 (8)	0.37 (2)
Si2	0.5092 (2)	0.15646 (7)	0.54632 (17)	0.0046 (7)	0.00065 (10)	0.0025 (4)	−0.00006 (8)	0.0024 (5)	−0.00005 (7)	0.42 (3)
O1	0.0000	0.0000	0.0000	0.013 (3)	0.0000 (4)	0.0062 (11)	−0.0001 (3)	0.0057 (15)	0.0002 (3)	0.87 (8)
O2	0.5000	0.1047 (3)	0.7500	0.010 (3)	0.0007 (4)	0.0040 (11)	0.0000	0.0054 (15)	0.0000	0.66 (7)
O3	0.2450 (6)	0.1333 (2)	0.9198 (5)	0.0037 (16)	0.0017 (3)	0.0037 (8)	−0.0001 (3)	0.0026 (10)	−0.0002 (3)	0.64 (5)
O4	0.3228 (6)	0.09946 (19)	0.3239 (5)	0.0066 (15)	0.0011 (3)	0.0046 (9)	−0.0004 (3)	0.0028 (11)	−0.0005 (3)	0.75 (5)
O5	0.0332 (6)	0.21241 (18)	0.4689 (5)	0.0057 (15)	0.0006 (3)	0.0066 (8)	0.0001 (3)	0.0044 (10)	0.0001 (3)	0.63 (6)

indices of the structure refinements performed with the higher pressure data or deviations or discontinuities in the unit-cell parameters (Angel et al. 2001b). We therefore conclude that the Si1–O1–Si1 linkage in coesite remains linear to the highest pressures achieved in this study.

The Si1–Si1 distance across O1 is the longest Si–Si distance in the coesite structure by approximately 0.07 Å at room pressure. This Si1–O1–Si1 linkage therefore appears to be under tension as a result of mutual repulsion between two semiclose-packed planes of oxygen atoms parallel to (010) (Fig. 3). Such repulsion would stretch the Si1–O1–Si1 links, which are the only links between these planes of oxygens, and keep them linear. Our structure refinements certainly show that the O3–O4 distance that represents the separation of these planes increases slightly with increasing pressure, and this would be a mechanism by which the Si1–O1–Si1 linkage (Fig. 3) is kept linear. However, the rigid-unit DLS simulations of the high-pressure structures actually show an even greater increase in the O3–O4 distance than is observed experimentally. Therefore any tension applied to the Si1–O1–Si1 linkage cannot arise from direct repulsion between O3 and O4, because such repulsions are not included in the simulation model. We can only conclude, as did Megaw (1970), that the linear Si1–O1–Si1 linkage appears instead to be a consequence of the connectivity of the tetrahedral framework.

The four other symmetrically distinct Si–O–Si angles all show a steady decrease with increasing pressure (Fig. 2), but the largest one, at the O4 atom, actually compresses less, rather than more, than the smaller angles at O3, O2 and O5 atoms. This pattern of angle changes corresponds to a rotation of the Si2 tetrahedron around the [001] direction, by a total of about 4° between room pressure and 8.7 GPa (Fig. 4). The DLS simulation undertaken with the rigid-unit model reproduces both this general compressional behaviour of the Si–O–Si angles (Fig. 2) and the rotation of the Si2 tetrahedron (Fig. 4). Therefore, we can conclude that the pattern of bond-angle compression itself is actually a consequence of the connectivity of the coesite framework. The differences between the Si–O–Si angles predicted in the simulation and those actually observed can

Table 3 Bond lengths and angles in coesite at high pressure

	X1air 10^{-4}	X1P0 10^{-4}	X1P8 2.248(6)	X4P4 2.84(4)	X1P3 3.763(5)
Si2–O2–Si2	142.69(11)	142.53(24)	139.93(24)	139.17(20)	138.43(24)
Si1–O3–Si2	144.48(9)	144.84(14)	143.40(15)	142.34(17)	142.20(15)
Si1–O4–Si2	149.61(8)	149.75(17)	149.52(18)	149.68(15)	149.07(18)
Si1–O5–Si2	137.44(8)	137.38(14)	135.01(14)	134.64(17)	133.74(13)
Si1–O1	1.5949(4)	1.5953(9)	1.5860(9)	1.5853(8)	1.5820(10)
Si1–O3	1.6135(11)	1.6059(22)	1.6056(22)	1.6072(22)	1.6053(22)
Si1–O4	1.6110(13)	1.6077(21)	1.6045(21)	1.6040(26)	1.6047(21)
Si1–O5	1.6198(12)	1.6268(26)	1.6178(25)	1.6243(24)	1.6169(25)
Average	1.610	1.609	1.603	1.605	1.602
O1–Si1–O3	110.39(5)	110.60(10)	110.61(10)	110.39(9)	110.55(9)
O1–Si1–O4	109.33(5)	109.40(10)	108.38(10)	108.33(9)	107.71(11)
O1–Si1–O5	109.98(5)	109.94(9)	109.80(9)	109.94(11)	109.94(9)
O3–Si1–O4	110.32(7)	110.25(11)	110.73(11)	111.02(14)	110.93(11)
O3–Si1–O5	107.80(6)	107.78(12)	108.02(12)	107.75(11)	108.06(12)
O4–Si1–O5	108.99(6)	108.84(12)	109.29(13)	109.39(12)	109.65(12)
Si2–O2	1.6115(7)	1.6105(14)	1.6055(14)	1.6075(13)	1.6032(15)
Si2–O3	1.6137(12)	1.6179(21)	1.6122(19)	1.6126(25)	1.6096(20)
Si2–O4	1.6052(13)	1.6089(21)	1.6047(20)	1.5989(26)	1.5995(21)
Si2–O5	1.6164(12)	1.6083(28)	1.6205(27)	1.6128(22)	1.6167(28)
Average	1.612	1.611	1.611	1.608	1.607
O2–Si2–O3	109.65(5)	109.87(9)	109.83(11)	109.50(10)	109.75(10)
O2–Si2–O4	109.33(6)	109.40(11)	109.36(11)	109.39(11)	109.36(11)
O2–Si2–O5	110.33(7)	110.40(15)	110.35(15)	110.41(12)	110.15(14)
O3–Si2–O4	108.86(7)	108.52(13)	108.76(12)	109.02(12)	108.69(11)
O3–Si2–O5	109.36(6)	109.41(11)	109.23(10)	109.26(12)	109.14(10)
O4–Si2–O5	109.27(7)	109.21(13)	109.30(12)	109.24(13)	109.73(13)

be attributed to the effects of compression mechanisms not included in the simulations. These are specifically the compressibility of the Si–O bonds, and the internal deformation of the tetrahedra.

The reason for the success of a rigid-unit DLS simulation in describing the compression of coesite rests in the observation that neither of the two symmetrically distinct SiO_4 tetrahedra undergoes a large amount of deformation, at least to 8.7 GPa. Indeed, the Si2 tetrahedron shows very little internal deformation and the most compressible bond, Si2–O4, undergoes only 1.4% shortening. The Si1–O1 bond shortens by a similar amount, 1.6%. Note that this does not contradict the observation of the expansion of the (010) semiclose-packed layers that the Si1–O1–Si1 bridges (Fig. 3), but is achieved by rotation of the Si1–Si1 vector towards the (010) plane normal.

The Si1 tetrahedron is more distorted at room pressure than the Si2 tetrahedron, and then undergoes significantly more internal deformation than the Si2 tetrahedron as the pressure is increased. The O1–Si1–O4 angle decreases by $\sim$3.5° while the O4–Si1–O3 and O4–Si1–O5 angles increase by a similar amount (Table 3). The deformation can therefore be considered in terms of a rotation of the Si1–O4 bond towards the Si1–O1 bond. The internal deformation of the Si1 tetrahedra appears to be a consequence of the connectivity of the framework. The Si1 tetrahedron is connected to three Si2 tetrahedra via shared O3, O4 and O5 oxygen atoms. Examination of Figure 4 shows that a rigid rotation of these three Si2 tetrahedra can only be accommodated by a distortion of the Si1 tetrahedron. The distortion is enhanced by the compression of the Si1–O1 bond while the separation of the O3,O4 close-packed planes is increased. The question as to why the deformation is restricted to the Si1 tetrahedron, instead of being distributed over both tetrahedra, remains open; the same pattern of deformation and angle changes are also apparent in the most recent first-principles calculations of coesite at high pressure (Gibbs et al. 2000).

Elastic properties and structure

The rotation of the Si2 tetrahedron provides the key to relating the elastic properties of coesite to the structural changes that accompany compression. First, the anisotropy of compression of coesite, and its similarity to that observed in feldspars (e.g. Angel 1994), has been attributed to the channels parallel to [001] within the structure. In feldspars these channels are occupied by the extra-framework cations such as Na, K, Ca etc., but they are empty in coesite. Approximately 60% of the volume compression in both coesite and all feldspar structures is accommodated by compression along the (100) plane normal, perpendicular to these channels.

Table 3 (Contd.)

X4P2 4.45(4)	X4P3 5.01(4)	X1P12 6.16(4)	X1P5 6.509(6)	X1P7 7.814(11)	X4P1 8.68(4)
137.60(22)	137.23(19)	135.76(25)	135.86(25)	134.84(24)	133.78(21)
141.49(49)	141.09(17)	140.17(16)	140.08(16)	139.25(15)	138.47(20)
149.08(17)	148.88(15)	149.23(19)	148.88(20)	148.87(19)	148.40(17)
133.63(19)	133.29(17)	132.17(14)	131.72(14)	131.15(14)	130.57(19)
1.5809(9)	1.5793(8)	1.5733(9)	1.5746(9)	1.5699(10)	1.5686(9)
1.6033(25)	1.6015(22)	1.6073(25)	1.6052(23)	1.6061(23)	1.6039(24)
1.5996(29)	1.6014(26)	1.6002(24)	1.6040(23)	1.5964(23)	1.5965(31)
1.6210(25)	1.6191(23)	1.6083(25)	1.6120(27)	1.6140(26)	1.6116(26)
1.601	1.600	1.597	1.599	1.597	1.595
110.37(10)	110.44(9)	110.45(10)	110.35(10)	110.42(10)	110.21(10)
107.59(10)	107.23(9)	107.11(11)	106.80(11)	106.56(11)	106.13(10)
110.17(12)	110.26(11)	110.05(9)	110.07(9)	110.21(10)	110.14(12)
111.13(15)	111.21(14)	111.30(12)	111.50(13)	111.57(11)	111.89(17)
107.86(12)	107.90(11)	107.86(13)	108.30(13)	107.87(12)	107.95(12)
107.86(12)	109.81(11)	110.08(12)	109.82(13)	110.23(13)	110.53(13)
1.6054(14)	1.6024(12)	1.6020(17)	1.6006(16)	1.5982(17)	1.6008(15)
1.6137(28)	1.6146(26)	1.6078(21)	1.6070(22)	1.6062(22)	1.6078(31)
1.5979(28)	1.5966(26)	1.5933(24)	1.5907(23)	1.5918(23)	1.5873(31)
1.6072(24)	1.6070(22)	1.6194(29)	1.6147(31)	1.6108(28)	1.6117(24)
1.606	1.605	1.606	1.603	1.602	1.602
109.42(12)	109.42(10)	109.21(11)	109.27(11)	109.18(11)	108.85(12)
109.40(12)	109.53(11)	109.51(12)	109.36(13)	108.93(12)	109.39(12)
110.34(14)	110.32(12)	110.83(14)	110.36(15)	110.69(14)	110.97(13)
108.74(13)	108.69(12)	108.88(12)	108.94(12)	108.93(12)	108.98(14)
109.08(12)	108.90(11)	108.84(11)	109.16(12)	108.86(11)	108.87(13)
109.82(14)	109.97(13)	109.54(13)	109.73(13)	109.55(14)	109.74(16)

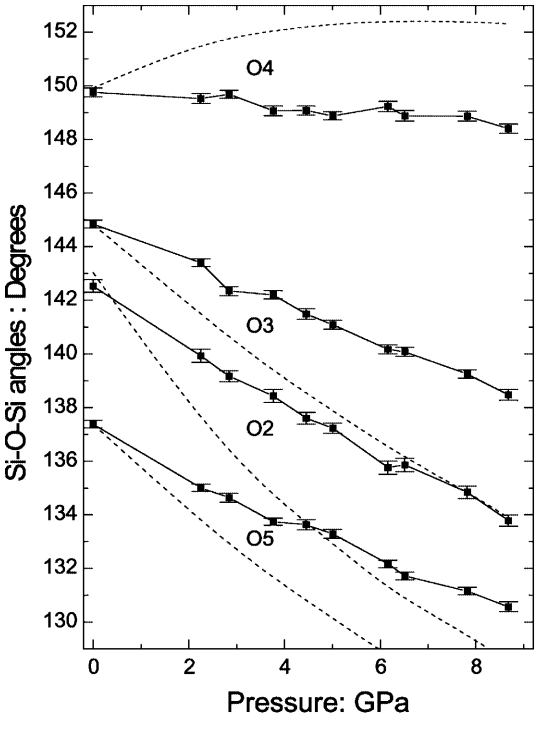

Fig. 2 The variation of the Si–O–Si bond angles in coesite with pressure. *Symbols with error bars* are experimental data. *Broken lines* are the angles predicted by the rigid-unit DLS model

However, simple compression of the width of the channels alone does not occur, because they are bridged by 4-rings of tetrahedra to form the crankshaft chains present in both structures. The rotation of the Si2 tetrahedra about [001] in coesite leads to a shearing of the 4-rings as indicated by the changes in O–O distances that comprise the diagonals of the rings (Fig. 5). The changes in the O–O distances across the channels (Fig. 6) also reflect this pattern of shear. Taken alone, the shearing clearly leads to a decrease in the size of the unit cell along the (100) plane normal, an increase in the [001] direction and an increase in the β unit-cell angle. The shear therefore contributes to a soft (100) and a stiff [001] direction, as observed. The counter-rotation of consecutive Si2 tetrahedra joined by the common O2 oxygen atom (Fig. 5) also increases the torsion angle between them. Therefore the Si2–Si2 distance must decrease in order to prevent the Si2–O2–Si2 angle from increasing thereby, making a further small, but opposite, contribution to the compression of the *c*-cell edge.

The rigid-unit DLS simulation provides a possible reason for the stiffening of the structure with increasing pressure, as measured by the positive value of K″. The simulation predicts a limit to the expansion of the Si1–O4–Si2 angle around 3 GPa. One might speculate that, at higher pressures, the continued rotation of the Si2 tetrahedra is achieved in the real structure by the initi-

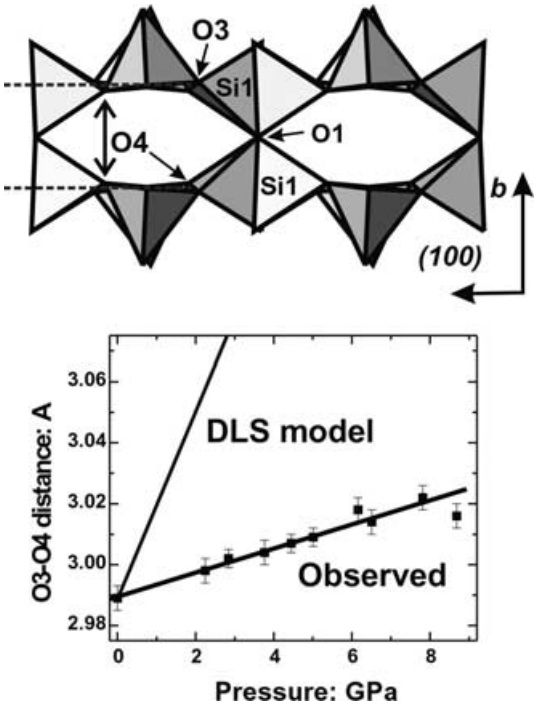

Fig. 3 A polyhedral representation of the room-pressure coesite structure viewed down the *c*-cell edge. Two adjacent semiclose-packed planes of O3 and O4 oxygen atoms parallel to (010) are indicated by the *dashed lines*. The linear Si1–O1–Si1 linkages are the only bridges between these two adjacent planes. The measured evolution of the separation of these planes with pressure, as measured by the O3–O4 distance, is shown in the *lower part of the figure*, along with that predicted by the rigid-unit DLS model

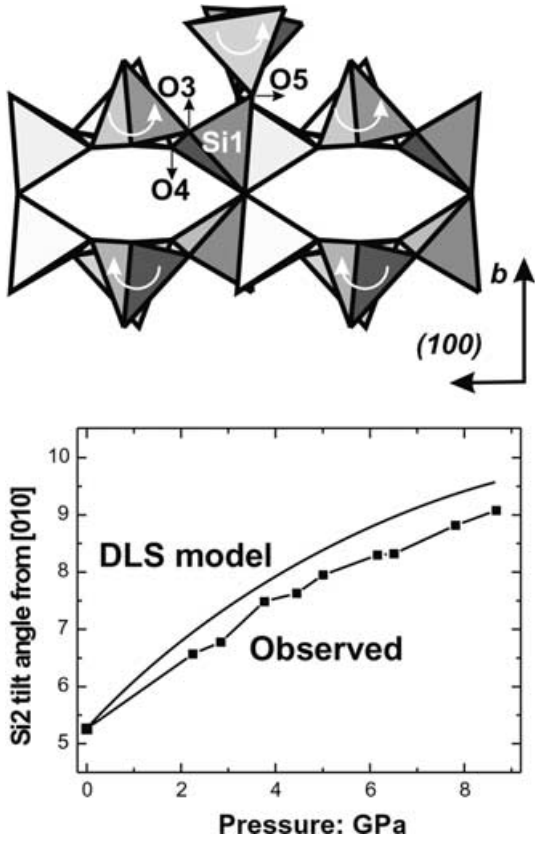

Fig. 4 A polyhedral representation of the coesite structure determined at 8.68 GPa viewed down the *c*-cell edge. Note that the rotation around [001] with pressure (*white arrows*) is apparent in the increased separation of the O5 apices compared to the room pressure structure shown in Fig. 3. The tilt of Si2 is quantified as the angle between the O3–O4 vector within a tetrahedron and the (010) plane. The measured evolution of this angle with pressure is shown in the *lower part of the figure*, along with that predicted by the rigid-unit DLS model. This rotation of the Si2 tetrahedra moves the O3, O4 and O5 oxygen atoms as indicated by the *black arrows* and imposes a distortion on the Si1 tetrahedra

ation of further, presumably stiffer, mechanisms of compression. A comparison of the observed Si–Si distances with those calculated from the observed Si–O–Si angles but the room pressure Si–O distances suggests that one of these changes is the initiation of significant compression of the Si–O5 distances above 3 GPa (Fig. 7). Furthermore, the two most compressible O5–O5 distances across the [001] channels within the structure show significant stiffening at higher pressures (Fig. 6) that presumably also contributes to the positive value of K″.

The s_{23} component of the elastic compliance tensor cannot be separately measured in a purely hydrostatic compression experiment. We therefore performed further DLS calculations in order to simulate the effect of uniaxial stress upon the coesite framework. After initial relaxation of the model structure, stress was simulated by simply fixing the *b* unit-cell parameter at a series of values while the remaining cell parameters and the atom coordinates were relaxed subject to the rigid-body constraints described in the experimental section. These simulations showed that reduction of the *b* unit-cell parameter led to a linear response of the coesite structure at least for up to −1.4% imposed linear strain (Fig. 8). The *d*(100) spacing expands by 0.66% and the *c*-cell edge is shortened by 0.05% for 1% linear strain applied along [010]. The latter implies directly that this simulation model possesses a negative value of s_{23}, as does coesite. Furthermore, the ratio of the expansion and compression predicted by this simplistic DLS model, $\varepsilon_1/\varepsilon_3 = -13$, is of the same order of magnitude as the value of −21 calculated from the measured elastic constants of coesite (Weidner and Carleton 1977). Similarly, the measured elastic constants would predict a ratio of linear strains $\varepsilon_1/\varepsilon_2 = -17.5$ for uniaxial compression of the *c*-cell edge, while the DLS simulation yields a ratio of −10.

It therefore appears that the anomalous positive values of both s_{23} and K in the equation of state of coesite, its high elastic anisotropy and the unusual straight Si1–O1–Si1 linkage within the structure are simply consequences of the specific connectivity of the tetrahedral framework comprising the coesite structure. That the properties are a consequence of framework connectivity and not the specific symmetry is supported

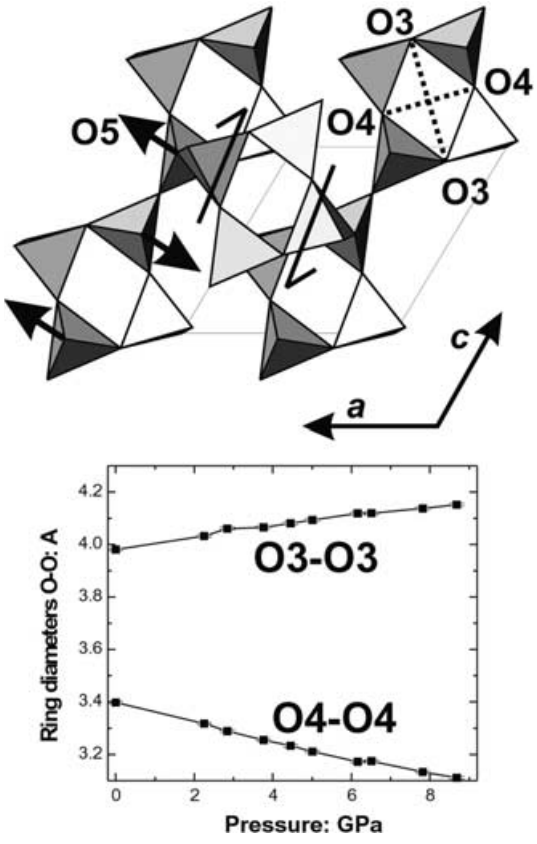

Fig. 5 A polyhedral representation of part of the room-pressure coesite structure viewed down the *b*-cell edge. As pressure increases the Si2 tetrahedra tilt as indicated by the *full arrows*, leading to an increase in the O3–O3 distances and decrease in O4–O4 distances across the 4-rings that bridge the [001] channels within the structure. These changes comprise a shear of the structure as indicated by the *half arrows*. The shear by itself would contribute to compression of the (100) plane normal and expansion along [001]

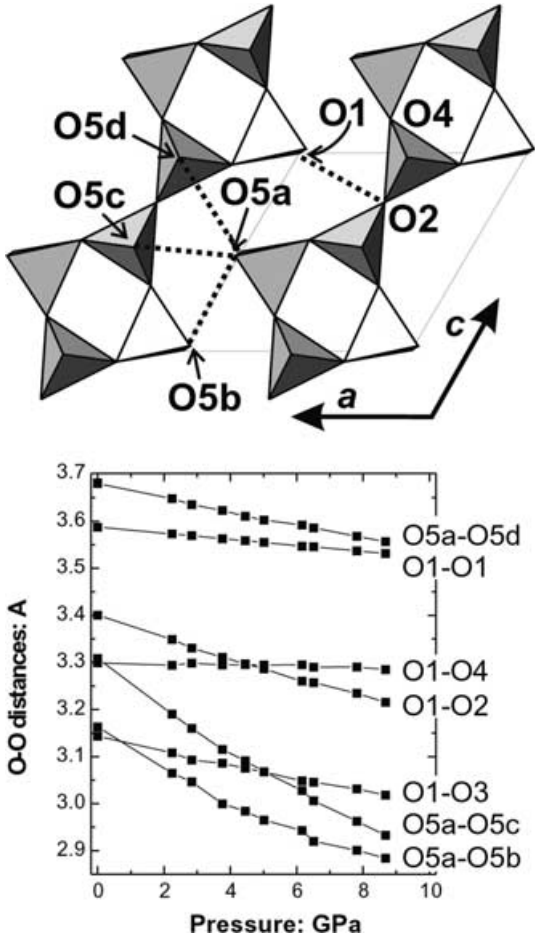

Fig. 6 A polyhedral representation of a single layer of the room-pressure coesite structure viewed down the *b*-cell edge. As pressure increases the O–O distances across the [001] channels decrease in a manner that reflects the shear of the overlying 4-rings that are shown in Fig. 5. The distances undergoing the largest changes are indicated by *dashed lines*; note that the O5a–O5b distance, which undergoes the greatest compression, shows signs of significant stiffening at higher pressures. The esd of the O–O distances is smaller than the symbol size in the graph

by data on other polymorphs of silica. Cristobalite has a negative bulk Poisson ratio in both its tetragonal and cubic phases (Yeganeh-haeri et al. 1992; Kimizuka et al. 2000) that can also be explained in terms of the behaviour of rigid SiO_4 tetrahedra (Alderson and Evans 2001). In contrast, both the trigonal and hexagonal phases of quartz have a positive Poisson ratio (e.g., Carpenter et al. 1998).

Acknowledgements The help of Christian Baerlocher of ETH Zurich in providing both the DLS-76 software and advice in its use is gratefully acknowledged, as are discussions with Paul Ribbe of Virginia Tech and the comments of two anonymous reviewers. The data analysis was supported by the National Science Foundation under grant EAR-0105864 to N.L. Ross and R.J. Angel.

References

Abrahams S, Keve E (1971) Normal probability plot analysis of error in measured and derived quantities and standard deviations. Acta Crystallogr (A) 27: 157–165

Alderson A, Evans KE (2001) Rotation and dilation deformation mechanisms for auxetic behaviour in the alpha-cristobalite tetrahedral framework structure. Phys Chem Miner 28: 711–718

Allan DR, Miletich R, Angel RJ (1996) A diamond-anvil cell for single-crystal X-ray diffraction studies to pressures in excess of 10 GPa. Rev Sci Instrum 67: 840–842

Angel RJ (1994) Feldspars at high pressure. In: Parsons I (ed) Feldspars and their reactions. Kluwer Academic, Dordrecht, pp 271–312

Angel RJ (2003) Automated profile analysis for single-crystal diffraction data. J Appl Crystallogr in press

Angel RJ (2003). Software for single-crystal data reduction. http://www.crystal.vt.edu/crystal/

Angel RJ, Allan DR, Miletich R, Finger LW (1997) The use of quartz as an internal pressure standard in high-pressure crystallography. J Appl Crystallogr 30: 461–466

Angel RJ, Downs RT, Finger LW (2001a) High-pressure, high-temperature diffractometry. In: Hazen RM, Downs RT (eds) High-pressure, high-temperature crystal chemistry, MSA pp 559–596

Angel RJ, Mosenfelder JL, Shaw CSJ (2001b) Anomalous compression and equation of state of coesite. Phys Earth Planet Int 124: 71–79

Baerlocher C, A. H, Meier W (1977). DLS-76 A program for the simulation of crystal structures by geometric refinement. http://www.kristall.ethz.ch/LFK/software/xrs/dls76.html

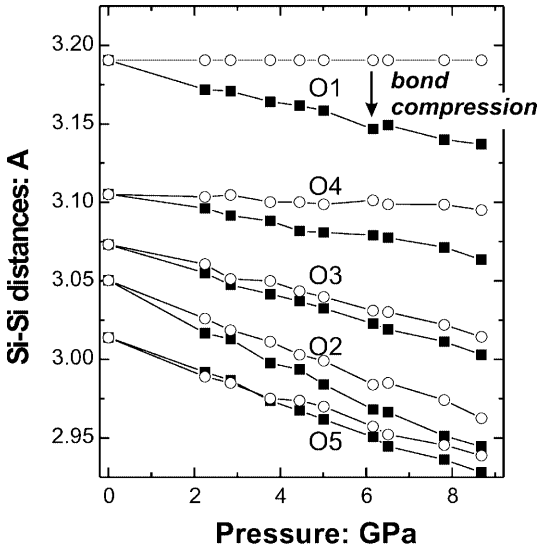

Fig. 7 The variation of the Si–Si distances in coesite with pressure. The *filled symbols* are the experimental data. The esd is smaller than the symbol size in the graph. The open symbols are the Si–Si distances calculated for the Si–O–Si angles at each pressure and the Si–O distances at room pressure. The difference between the observed and calculated distances therefore represents the contribution of Si–O bond compression to the reduction in Si–Si distances. This difference is greatest for Si1–Si1 because the Si1–O1–Si1 angle is constrained to 180° and reduction in Si1–Si1 is only due to the compression of Si1–O1. For the O2, O3 and O5 linkages the results suggest that bond compression is initiated from room pressure, but significant bond compression in the Si1–O5–Si2 link only seems to start at pressures of ~3 GPa

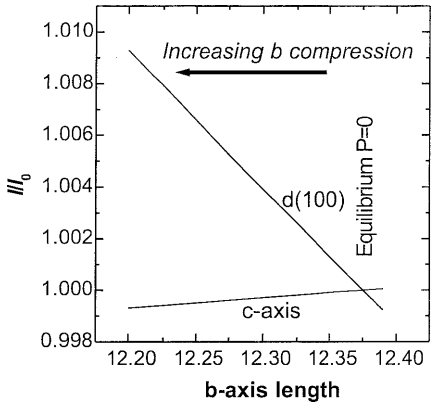

Fig. 8 The variation of $d(100)$ and the c unit-cell parameter in a rigid-unit DLS simulation of the structure of coeste at room pressure. The increase in $d(100)$ as the b-cell edge is compressed indicates that the s_{23} element of the elastic compliance tensor is negative

Becker P, Coppens P (1974) Extinction within the limit of validity of the Darwin transfer equations. I. General formalisms for primary and secondary extinction and their application to spherical crystals. Acta Crystallogr (A) 30: 129–147

Burnham CW (1966) Computation of absorption corrections and the significance of end effects. Am Mineral 51: 159–167

Carpenter MA, Salje EKH, Graeme-Barber A, Wruck B, Dove MT, Knight KS (1998) Calibration of excess thermodynamic properties and elastic constant variations associated with the alpha < − >beta phase transition in quartz. Am Mineral 83: 2–22

Chopin C (1983) High-pressure facies series in pelitic rocks: a review. Terra Cognita 3: 183

Creagh D, McAuley W (1992) X-ray dispersion correction. In: Wilson A (ed) International Tables for X-ray Crystallography, vol C, Kluwer Academic, Dordrecht, pp 206–219

Downs JW (1995) Electron density and electrostatic potential of coesite. J Phys Chem 99: 6849–6856

Finger L, Prince E (1974). A system of Fortran-IV computer programs for crystal structure computations

Finger LW, King H (1978) A revised method of operation of the single-crystal diamond cell and refinement of the structure of NaCl at 32 kbar. Am Mineral 63: 337–342

Geisinger KL, Spackman MA, Gibbs GV (1987) Exploration of structure, electron-density distribution, and bonding in coesite with Fourier and pseudo-atom refinement methods using single-crystal X-ray diffraction data. J Phys Chem 91:3237–3244

Gibbs GV, Boisen MB, Rosso KM, Teter DM, Bukowinski MST (2000) Model structures and electron density distributions for the silica polymorph coesite at pressure: an assessment of OO bonded interactions. J Phys Chem (B) 104: 10534–10542

Grandinetti PJ, Baltisberger JH, Farnan I, Stebbins JF, Werner U, Pines A (1995) Solid-state O-17 magic-angle and dynamic-angle spinning NMR study of the SiO_2 polymorph coesite. J Phys Chem 99: 12341–12348

Kimizuka H, Kaburaki H, Kogure Y (2000) Mechanism for negative Poisson ratios over the alpha–beta transition of cristobalite, SiO_2: a molecular-dynamics study. Phys Rev Lett 84: 5548–5551

King H, Finger LW (1979) Diffracted beam crystal cenetering and its application to high-pressure crystallography. J Appl Crystallogr 12: 374–378

Levien L, Prewitt CT (1981) High-pressure crystal structure and compressibility of coesite. Am Mineral 66: 324–333

Maslen E, Fox A, O'Keefe M (1992) X-ray scattering. In: Wilson A (ed) International tables for X-ray crystallography, vol C, Kluwer Academic, Dordrecht, pp 476–509

Megaw H (1970) Structural relationship between coesite and feldspar. Acta Crystallogr (B) 26: 261–265

O'Brien PJ, Zotov N, Law R, Khan MA, Jan MQ (2001) Coesite in Himalayan eclogite and implications for models of India-Asia collision. Geology 29: 435–438

Parkinson CD (2000) Coesite inclusions and prograde compositional zonation of garnet in whiteschist of the HP-UHPM Kokchetav massif, Kazakhstan: a record of progressive UHP metamorphism. Lithos 52: 215–233

Parkinson CD, Katayama I (1999) Present-day ultrahigh-pressure conditions of coesite inclusions in zircon and garnet: evidence from laser Raman microspectroscopy. Geology 27: 979–982

Ralph R, Finger LW (1982) A computer program for refinement of crystal orientation matrix and lattice constants from diffractometer data with lattice symmetry constraints. J Appl Crystallogr 15: 537–539

Swainson IP, Dove MT (1995) Molecular-dynamics simulation of alpha-cristobalite and beta-cristobalite. J Phys: Condens Matter 7: 1771–1788

Weidner DJ, Carleton HR (1977) Elasticity of coesite. J Geophys Res 82: 1334–1346

Yeganeh-Haeri A, Weidner DJ, Parise JB (1992) Elasticity of alpha-cristobalite – a silicon dioxide with a negative Poisson ratio. Science 257: 650–652